Low-Temperature Fracture Toughness of a Heat-Treated Mild Steel

C.C. Chama

Specimens from a 0.14% C mild steel were austenitized at 1000 °C for 1 h and thereafter furnace-cooled or isothermally transformed at 700 °C for 0.5, 2, and 8 h. The microconstituents present in the as-received material were ferrite and pearlite and their amounts did not substantially change even after heat treatment. The impact energy of the as-received and the furnace-cooled materials increased from 4 to 89 J and from 4 to 108 J, respectively, when the temperature was changed from -196 to 23 °C. For these materials, the failure mode was by ductile fracture at 0 and 23 °C and by quasicleavage fracture at -196 and -40 °C. The fracture toughness did not show any significant change with isothermal transformation time at 700 °C. The failure mode of the isothermally transformed materials was always by quasicleavage fracture.

Keywords

fracture toughness, heat-treated mild steels, low-temperature fracture, transition fracture modes

1. Introduction

THE performance of materials at low temperatures has long been of considerable interest because of the anomalous behavior at these conditions especially when strain rates are high. The effect of temperature on fracture behavior has been a subject of previous investigations (Ref 1-4). Most of these investigations have focused on the character of fatigue crack propagation because of the importance of this property. In materials under impact stress, fracture is by ductile rupture or cleavage. These two modes of fracture may sometimes occur concurrently, although different microstructural features are involved in bringing them about (Ref 5).

Cleavage fracture occurs when sections of a material, such as stopped slip band, twin, or dislocation array, undergo shear when the applied stress exceeds the strength. Consider a material with spherical or plate-shaped carbide particles containing crack nuclei (hatched section in Fig. 1a and b) of size r and X. A crack will propagate across the carbide-ferrite interface if the maximum principal tensile stress, σ, acting on the material exceeds the particle fracture strength, σ_f (Ref 6, 7). For a penny-shaped crack, the crack propagation criterion is (Ref 6):

$$\sigma_f = \left[\frac{\pi E \gamma_p}{2(1-\nu^2)r}\right]^{1/2} \quad \text{(Eq 1)}$$

where σ_f is the fracture strength, E is Young's modulus, γ_p is the surface energy, ν is Poisson's ratio, and r is the crack size. For a through-thickness crack, the crack propagation criterion is (Ref 6):

$$\sigma_f = \left[\frac{2E\gamma_p}{\pi(1-\nu^2)r}\right]^{1/2} \quad \text{(Eq 2)}$$

In the case of a through-thickness crack, $r = X/2$ for the Griffith crack propagation criterion to be valid. In steels, cleavage fracture will involve three steps (Ref 7): (1) crack initiation and propagation within carbide particles, (2) crack propagation across the carbide-ferrite interface, and (3) crack propagation across the ferrite-ferrite grain boundary, leading to cleavage fracture. Crack initiation occurs in specific locations such as tips of notches or inclusions, which are stress concentration points. Crack propagation will be more significant across regions of weakness such as grain or phase boundaries. Therefore, cleavage fracture usually occurs by crack propagation along well-defined paths which are grain or phase boundaries, such as the carbide-ferrite or ferrite-ferrite interfaces in Fig. 1.

Ductile fracture arises from the nucleation, growth, and coalescence of voids to form cracks. Void coalescence rate, $\dot{f}$, can be expressed as (Ref 8):

$$\dot{f} = \dot{f}_{\text{nucleation}} + \dot{f}_{\text{growth}} \quad \text{(Eq 3)}$$

The void coalescence rate is dependent on both the nucleation rate, $\dot{f}_{\text{nucleation}}$, and the growth rate, $\dot{f}_{\text{growth}}$, of individual voids. At elevated temperatures, the mobility of voids is higher, leading to increased coalescence and ductile fracture. The source of most voids are vacancies created by mobile dislocations (Ref 9) or the presence of tensile stresses in a material (Ref 9, 10). A correlation has been found between fracture stress and spacing among these voids (Ref 11). In general, the fracture stress increases with decreasing intervoid spacing. This is attributed to the impediment of dislocation motion by the closely spaced voids.

In iron and iron-binary alloys at very low temperatures, crack propagation rates can be divided into two stages (Ref 12). The initial stage involves a decrease in crack propagation rate at low temperature, which is attributed to lower dislocation velocities that retard striation formation or cyclic cleavage. As the temperature decreases below that of the ductile-brittle transi-

C.C. Chama, Department of Metallurgy and Mineral Processing, University of Zambia, P.O. Box 32379, 10101 Lusaka, Zambia.

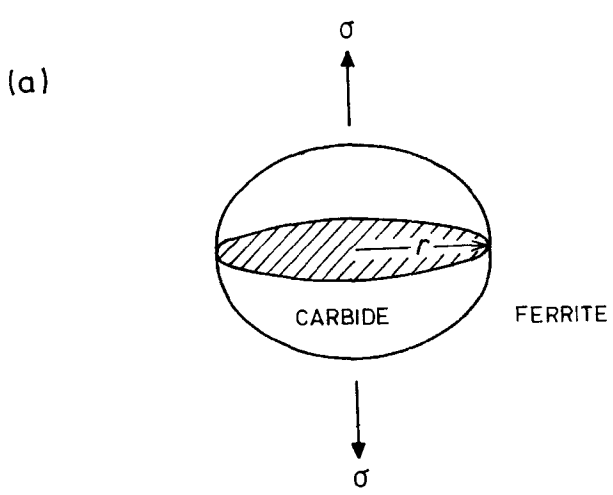

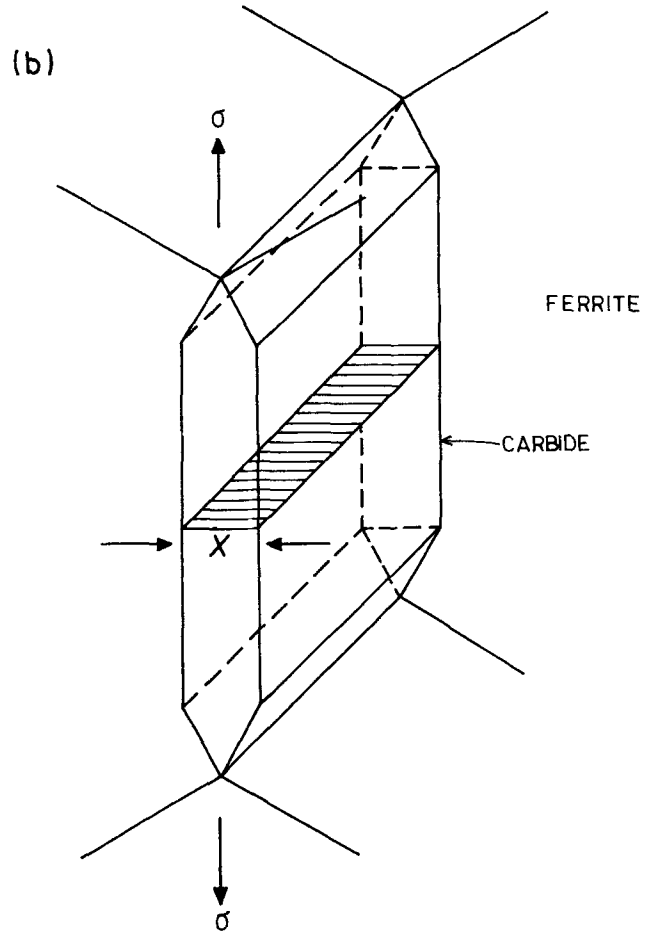

Fig. 1 (a) A penny-shaped crack nucleus in a spherical carbide particle. (b) A through-thickness crack nucleus in a plate-shaped grain boundary carbide particle (Ref 6)

tion, crack growth rates increase. The transition temperature can be expressed as (Ref 13):

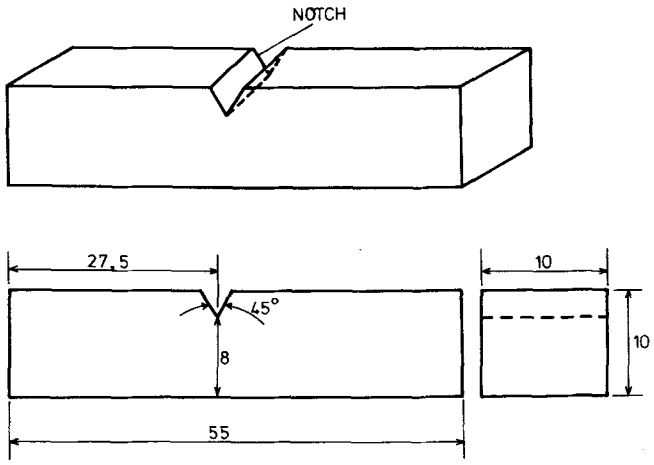

Fig. 2 Charpy impact test specimen (all dimensions are in mm)

$$ITT = 63 + 44.1(\%Si) + 2.2(\%pearlite) - 258(\%Al) - 2.3d^{-1/2} \quad \text{(Eq 4)}$$

where ITT is impact transition temperature and d is grain size. Equation 4 shows that the transition temperature is dependent on both composition and grain size, parameters that can be controlled by heat treatment. Although other investigators have reported fracture toughness measurements using Charpy impact tests, this article contributes additional information on the subject.

2. Experimental Procedures

The as-received composition of the investigated steel, in wt%, was 0.33 Si, 0.058 Al, 0.74 Mn, 0.019 Cu, 0.017 S, 0.019 P, 0.14 C, bal Fe. Additional investigations were conducted after subjecting specimens of this steel to one of the following heat treatment schemes:

- Austenitizing at 1000 °C for 1 h followed by furnace cooling
- Austenitizing at 1000 °C for 1 h followed by isothermal transformation at 700 °C for 0.5, 2, and 8 h and quenching in cold water

The microstructures were examined in a Neophot 30 optical microscope and quantitative microscopy was conducted in a Leitz CBA 8000 image analyzer. Specimens for fracture toughness measurements by Charpy impact tests were machined to the specifications shown in Fig. 2 before being tested in a Torsee Universal Pendulum Testing Machine TIT-30. The specimens were maintained at 23 °C, 0 °C (ice), –40 °C (dry ice and acetone), and –196 °C (liquid nitrogen) for 2 h prior to the tests. Each specimen was tested within 5 s after removal from the cooling environment. The fractographs from the Charpy impact tests were examined in a JEOL JSM-840A scanning electron microscope operating at 15 KV.

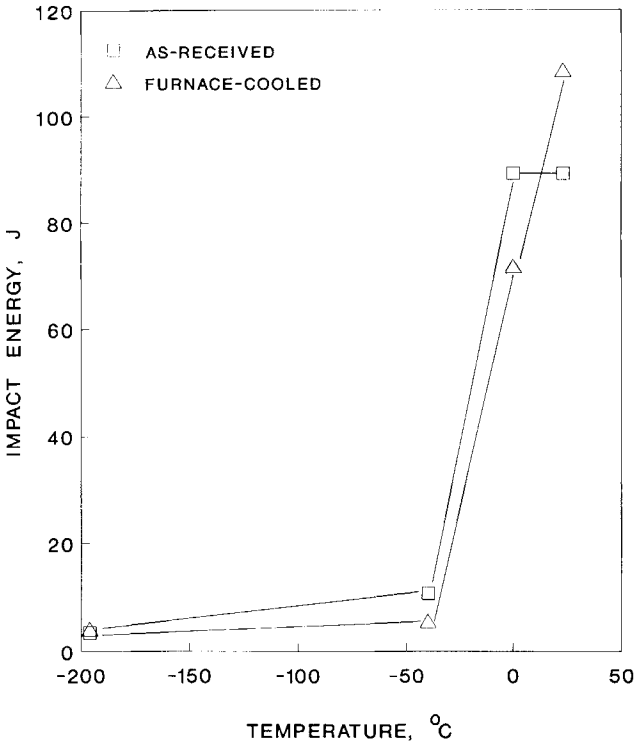

Fig. 3 Dependence of the fracture toughness on temperature of the as-received and furnace-cooled materials

3. Results and Discussion

3.1 *As-Received and Furnace-Cooled Materials*

The as-received and furnace-cooled materials both showed a decrease in impact energy when the temperature was lowered from 23 to –196 °C as shown in Fig. 3. For Fig. 3 and in all other cases, the impact data shown are averages obtained by conducting the tests on two specimens. At –196 °C, the impact energy of the as-received and furnace-cooled materials was about 4 J. At 23 °C, the impact energy was 89 and 108 J for the as-received and furnace-cooled materials, respectively. At 23 and 0 °C, fractographs from the as-received material had an extensive network of dimples, as shown in Fig. 4(a) and (b). At –40 °C, quasicleavage facets (A and B in Fig. 4c) appeared. The combination of very low temperatures and high triaxial stress to which a notch in the Charpy specimens is exposed can lead to cleavage fracture. At the lowest temperature, –196 °C, microvoids were present (arrows in Fig. 4d). Depending on their distribution, these microvoids may retard or increase crack growth (Ref 14).

The furnace-cooled material also revealed dimples at 23 °C (see Fig. 5a). At 0 °C, localized voids (around region A in Fig. 5b) and quasicleavage facets (region B) existed. Quasicleavage facets were also present in the materials tested at very low temperatures (–196 and –40 °C). Since the fractographs from the as-received and furnace-cooled materials tested at 23 °C had extensive dimples, it is likely that the failure mode at this temperature was dominated by ductile fracture. As stated above, ductile fracture involves three steps: void nucleation, growth, and coalescence. The presence of voids beyond a critical volume fraction has been shown to lower the stress required to induce deformation (Ref 15) because of the discontinuity that they introduce in the matrix. The failure mode at very low temperatures (–196 °C and –40 °C) was by quasicleavage fracture because of the relatively large amount of planar facets, as shown in the fractographs; cracks (arrows in Fig. 5c) and planes of shear during quasicleavage fracture (arrows in Fig. 5d) were quite apparent. There is evidence that under stress, cracks may grow by coalescence of adjacent cracks (Ref 16). It has previously been observed that at low temperatures, cracks can undergo unstable propagation by cracking of ferrite grains (Ref 17).

Table 1 Size of ferrite grains and pearlite colonies

Condition of material	Ferrite grain size, μm	Pearlite colony size, μm
As-received	19.4	29.0
Furnace-cooled	46.1	54.6
700 °C, 0.5 h	31.7	42.3
700 °C, 2 h	33.7	71.0
700 °C, 8 h	33.2	58.0

The microstructure of the as-received material had rolling textures (arrows in Fig. 6) in addition to pearlite colonies (e.g., region A) on ferrite grain boundaries. The furnace-cooled material also had rolling textures (arrows in Fig. 7). However, two important differences between the as-received and furnace-cooled materials can be noted. First, the pearlite colonies in the furnace-cooled material are almost twice as large as those in the as-received material (Table 1). Second, ferrite grain growth occurred in the furnace-cooled material as shown in Table 1. After austenitizing at 1000 °C and furnace cooling, the grain size increased by 138%.

3.2 *Materials Isothermally Transformed at 700 °C*

The materials that were isothermally transformed at 700 °C for 8 h had very low impact energy as compared to the as-received material at all temperatures except –196 °C (Fig. 8). At –196 °C, the impact energy was about 4 J for both the as-received material and the material isothermally transformed at 700 °C for 8 h. At 0 and 23 °C, the isothermally transformed material had a lower impact energy as compared to the furnace-cooled material (Fig. 3 and 8). No appreciable difference in fracture toughness existed at –196 and –40 °C. The furnace-cooled material had an impact energy range from 4 J at –196 °C to 108 J at 23 °C. On the other hand, the impact energy of the material isothermally transformed at 700 °C for 8 h varied only from 4 to 8 J over the same temperature range. The effect of isothermal transformation time at 700 °C on fracture toughness was also investigated and is shown in Fig. 9 for the specimens tested at –196, –40, 0, and 23 °C. An isothermal transformation time of zero hours in Fig. 9 refers to the as-received material. At 0 and 23 °C, there was about a 90% decrease in the impact energy after isothermal transformation (Fig. 9). At –40 °C, there was only a moderate decrease in impact energy after isothermal transformation. The impact energy was relatively constant for

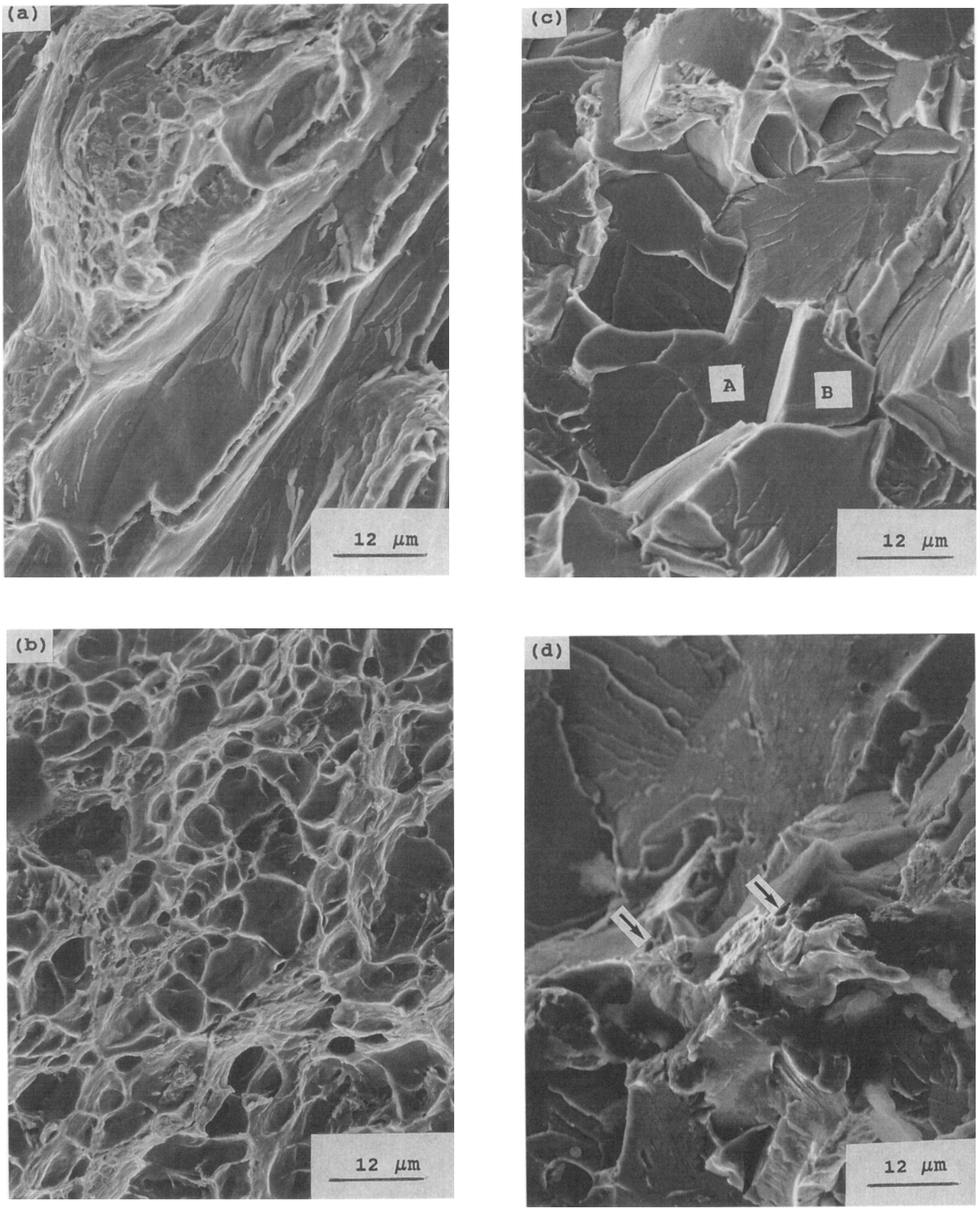

Fig. 4 Fractographs of the as-received material after Charpy impact tests at (a) 23 °C, (b) 0 °C, (c) –40 °C, and (d) –196 °C

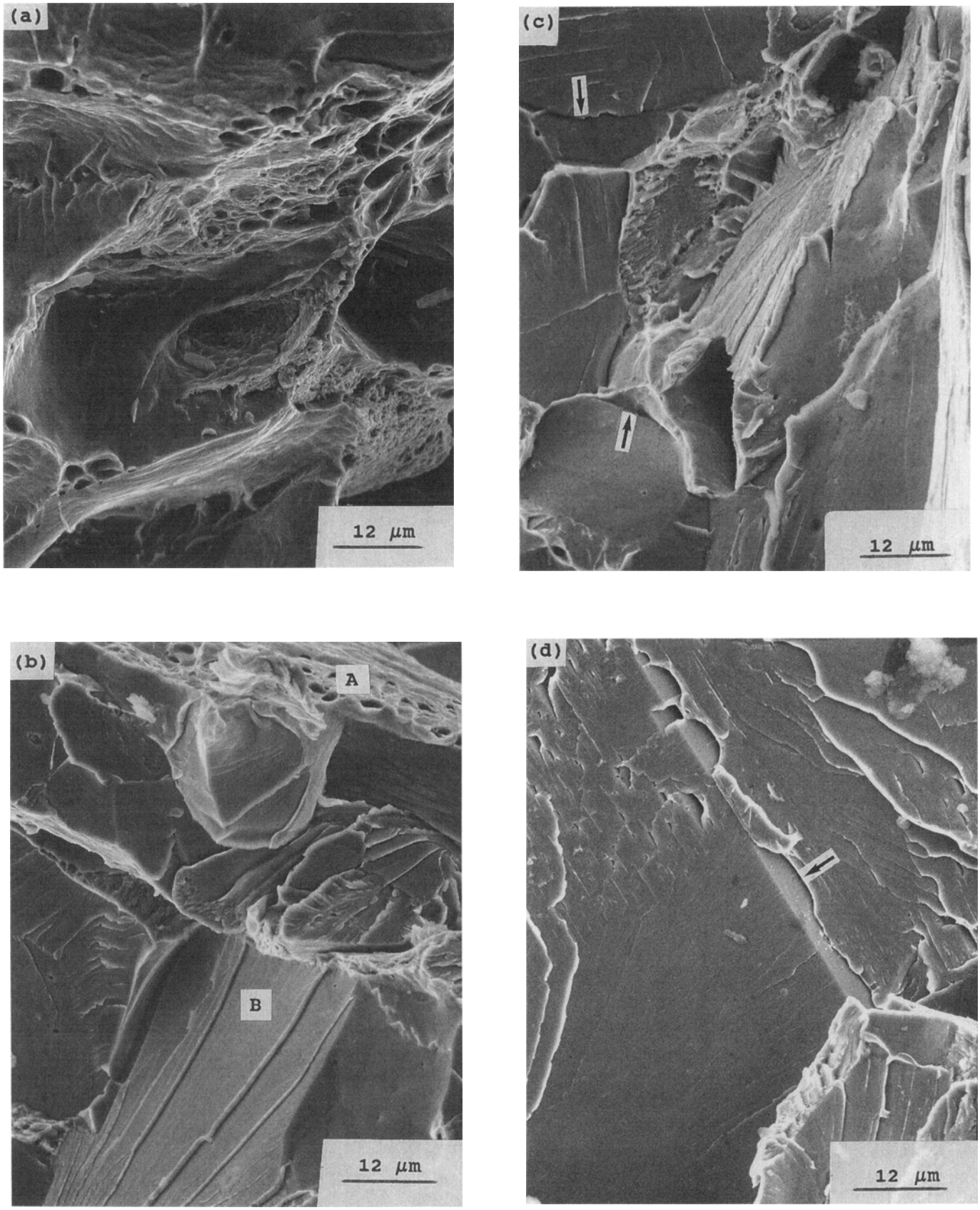

Fig. 5 Fractographs of the furnace-cooled material after Charpy impact tests at (a) 23 °C, (b) 0 °C, (c) –40 °C, and (d) –196 °C

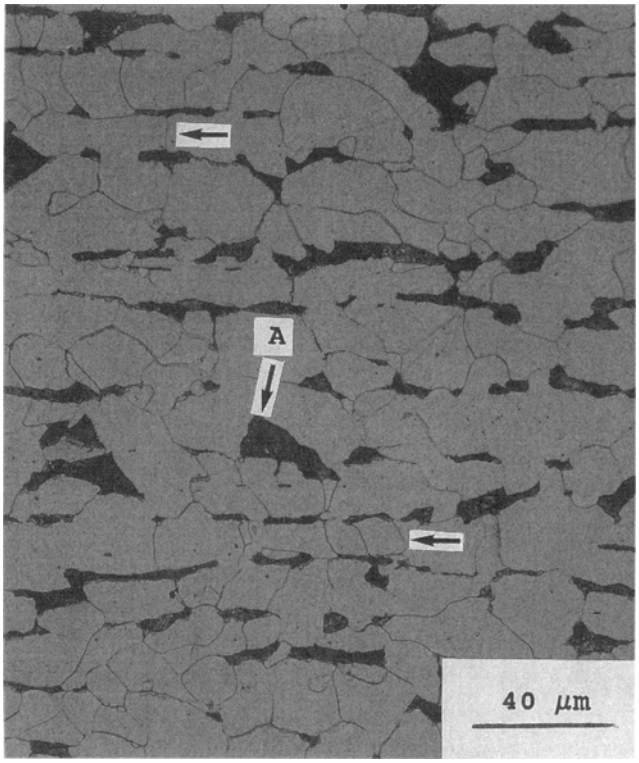

Fig. 6 Rolling textures and distribution of pearlite in the as-received material

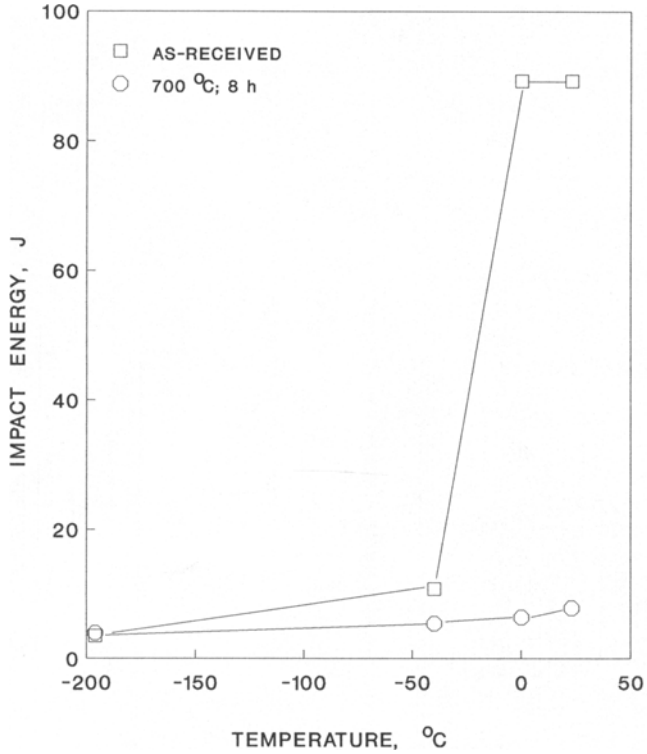

Fig. 8 Dependence of the fracture toughness on temperature of the as-received materials and samples that were isothermally transformed at 700 °C for 8 h

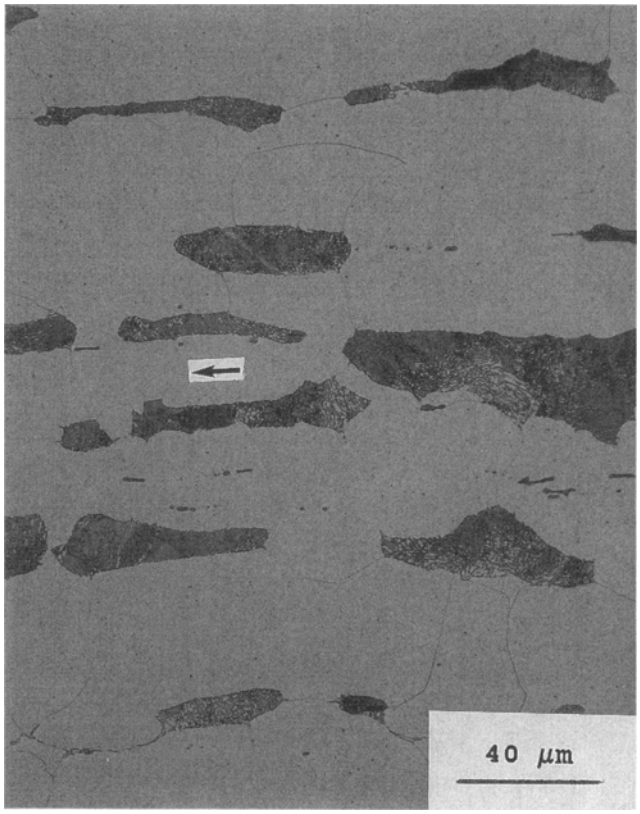

Fig. 7 Rolling textures and distribution of pearlite in the furnace-cooled material

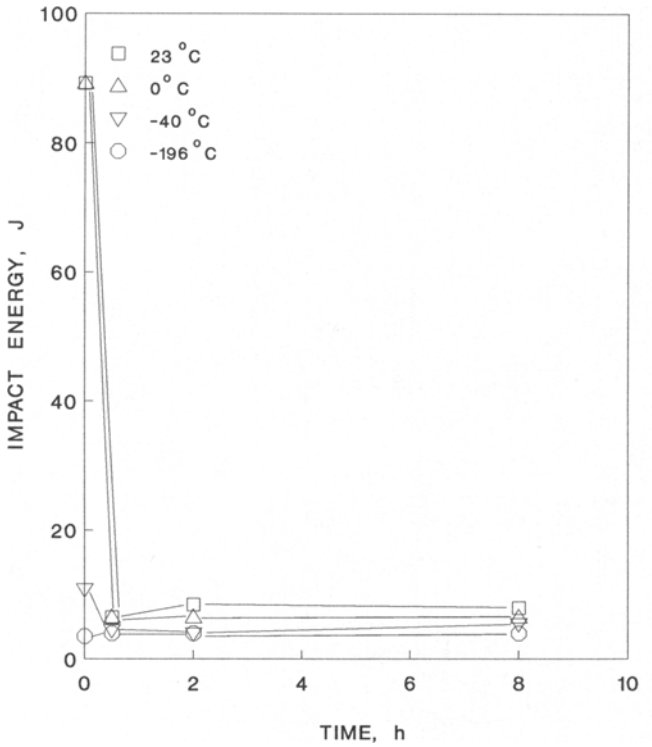

Fig. 9 Effect of isothermal transformation time on fracture toughness

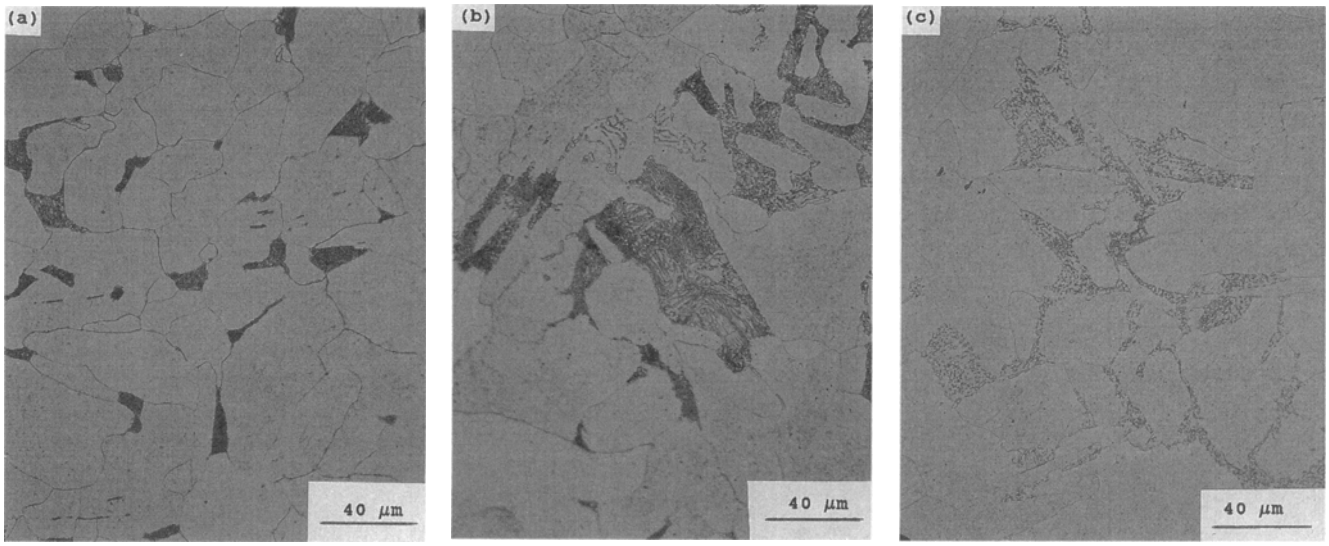

Fig. 10 Distribution of pearlite after isothermal transformation at 700 °C for (a) 0.5 h, (b) 2 h, and (c) 8 h

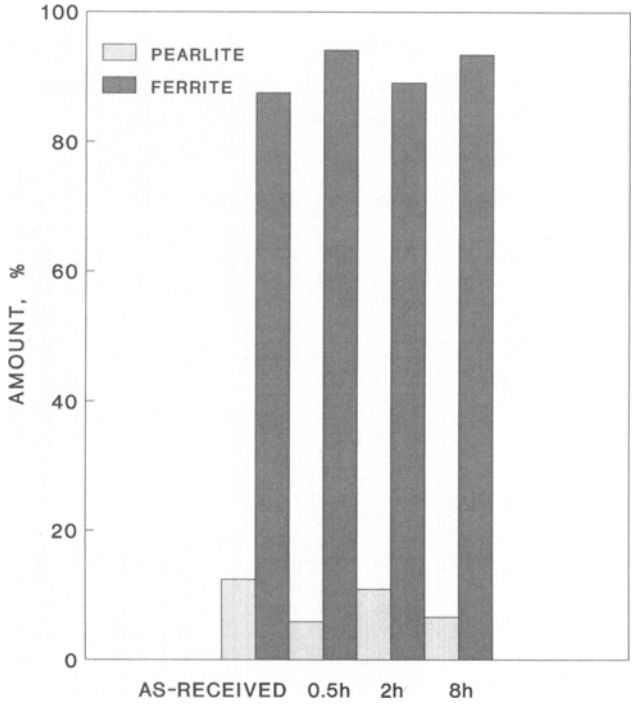

Fig. 11 Frequency distribution of pearlite and ferrite in the as-received material and samples that were isothermally transformed at 700 °C for 0.5, 2, and 8 h

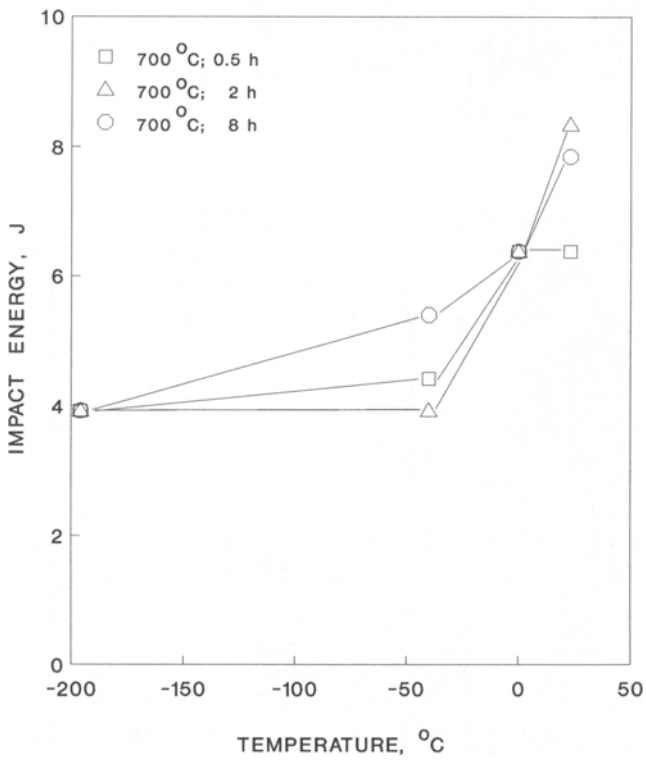

Fig. 12 Dependence of the fracture toughness on temperature of materials isothermally transformed at 700 °C

both the as-received and isothermally transformed materials when tested at −196 °C. At all temperatures the impact energy was relatively constant as the isothermal transformation time was changed from 0.5 to 8 h.

In the microstructure of the materials isothermally transformed at 700 °C for 0.5 h, pearlite existed on ferrite grain boundaries (Fig. 10a). After 2 h of isothermal transformation at 700 °C, there was a very significant increase in the size of the pearlite colonies (Table 1); the microstructure obtained is shown in Fig. 10(b). At a still longer isothermal transformation time of 8 h, partially spheroidized pearlite appeared along fer-

rite grain boundaries (Fig. 10c). After isothermal transformation at 700 °C, rolling textures were eliminated. This was probably due to recovery and recrystallization during isothermal transformation. At 700 °C, the ferrite grain size did not change with isothermal transformation time (Table 1). A histogram of the distribution of the microconstituents present is shown in Fig. 11. Twenty sets of data were obtained from each specimen and the calculated average values were used to construct the histogram. When the materials were isothermally transformed at 700 °C, the amounts of ferrite and pearlite did not really change with time and were about the same as in the as-received material.

For the isothermally transformed materials, the variation of the impact energy with temperature is shown in Fig. 12. In general, impact energy decreased with decreasing temperature from 23 to –196 °C. At 0 and –196 °C, the impact energy was the same irrespective of isothermal transformation time; there is no clear explanation for this. However, it should be noted that even at –40 and 23 °C, the differences in impact energy were negligible. Fractographs of materials that had been isothermally transformed at 700 °C for 0.5 h before testing are shown in Fig. 13. At 23 °C, the fractograph revealed the presence of many voids (e.g., regions A and B in Fig. 13a) in addition to quasicleavage facets (region C). As stated above, voids and facets are usually associated with ductile and cleavage fracture, respectively. The existence of both voids and quasicleavage facets indicates a mixed fracture mode. In a previous study on a steel containing 0.20% C (Ref 1), it was found that the fracture mode was usually mixed. At –196 °C, a mixture of intergranular and cleavage fracture was observed, whereas at 23 °C there was a mixture of ductile and intergranular fracture. Unlike the as-received and furnace-cooled materials, the specimens tested at 23 °C after isothermal transformation at 700 °C for 0.5 h did not contain a significant amount of dimples, which indicates that the failure mode was dominated by quasicleavage fracture. At 0 °C, striations (around region A in Fig. 13b) and planar quasicleavage facets (region B) were observed. At very low temperatures, a substantial amount of quasicleavage facets (regions A and B in Fig. 13c and d) were again present. Although transgranular fracture is associated with high impact energy, transgranular facets (region C in Fig. 13d) existed in the materials tested at –196 °C in spite of the low impact energy at this temperature. However, it is worth noting that the relative area of the fractograph associated with transgranular facets is smaller than that for the other modes of fracture. This shows that at –196 °C failure was not dominated by transgranular fracture.

At 23 °C, the materials isothermally transformed at 700 °C for 2 h revealed the presence of voids (e.g., region A in Fig. 14a) and cracks (region B). Cracks (arrows in Fig. 14b) were also observed after testing at 0 °C. As with the specimens isothermally transformed at 700 °C for 0.5 h, these materials had essentially no dimples. At –40 °C, transgranular facets (region A in Fig. 14c) existed in addition to quasicleavage facets (region B); a similar fractograph was obtained at –196 °C. The fractographs of the materials isothermally transformed at 700 °C for 8 h (Fig. 15) were similar to those in Fig. 14, with transgranular and quasicleavage facets coexisting after testing at –40 and –196 °C.

The dependence of fracture strength on ferrite grain size can be expressed as (Ref 7):

$$\sigma_f = \left[\frac{\pi E G_{ff}}{(1-\nu^2)\, d}\right]^{1/2} \quad \text{(Eq 5)}$$

in which G_{ff} is the dynamic strain energy release rate. For mild steel, $E = 210 \times 10^9$ Pa and $\nu = 0.29$. For example, using a G_{ff} value of 100 Jm^{-2} and a grain size of 19.4 μm (Table 1), the ferrite grain fracture strength of the as-received material as determined from Eq 5 is 1920 MPa. For the material isothermally transformed at 700 °C for 8 h, with a grain size of 33.2 μm, the ferrite grain fracture strength is 1470 MPa. Therefore, there is a moderate grain-size-dependent decrease in the fracture strength after isothermal transformation. Although these values of fracture strength are higher than what would normally be expected for mild steel, this does show, however, that grain size has some influence on fracture. The elements or compounds present in steel also influence the fracture behavior. There is evidence that phosphorus and sulfur have a significant effect on the fracture characteristics of steel (Ref 18, 19). When present, these elements may segregate to grain boundaries or, in the case of sulfur, form sulfides that are detrimental to the fracture strength of steel. The effect of segregation of phosphorus and sulfur was, however, not investigated in this study.

The actual mechanisms by which low temperatures degrade the fracture toughness of steel are still not very clear. However, it has been shown that the fracture toughness of steel is related to the size of carbide particles (Ref 20). In this case, temperature is believed to change the size of carbide particles, which, as mentioned above, act as nucleating sites for cracks. Perhaps even in the case of the 0.14% C mild steel used in this study, temperature affected fracture toughness by indirectly influencing some microstructural features.

4. Conclusions

The failure modes of a 0.14% C mild steel in the as-received and furnace-cooled conditions when tested at 0 and 23 °C is mostly by ductile fracture, whereas at –196 and –40 °C it is mostly by quasicleavage fracture. On the other hand, the failure mode in the materials austenitized at 1000 °C and thereafter isothermally transformed at 700 °C for 0.5, 2, and 8 h is by quasicleavage fracture at all test temperatures. Upon lowering of the temperature from 23 to –196 °C, the impact energy of the as-received material decreases from 89 to 4 J, and that of the furnace-cooled material decreases from 108 to 4 J. Furnace cooling of the 0.14% C mild steel from 1000 °C results in a moderate increase in fracture toughness only at 23 °C. On the other hand, the materials isothermally transformed at 700 °C for 0.5, 2, and 8 h have limited impact energy, and this falls within the range of only 4 to 8 J as the Charpy impact test temperature increases from –196 to 23 °C. At –196 °C the impact energy is 4 J for the as-received, furnace-cooled, and isothermally transformed materials. The amounts of ferrite and pearlite present in the as-received material do not change substantially even after isothermal transformation. However,

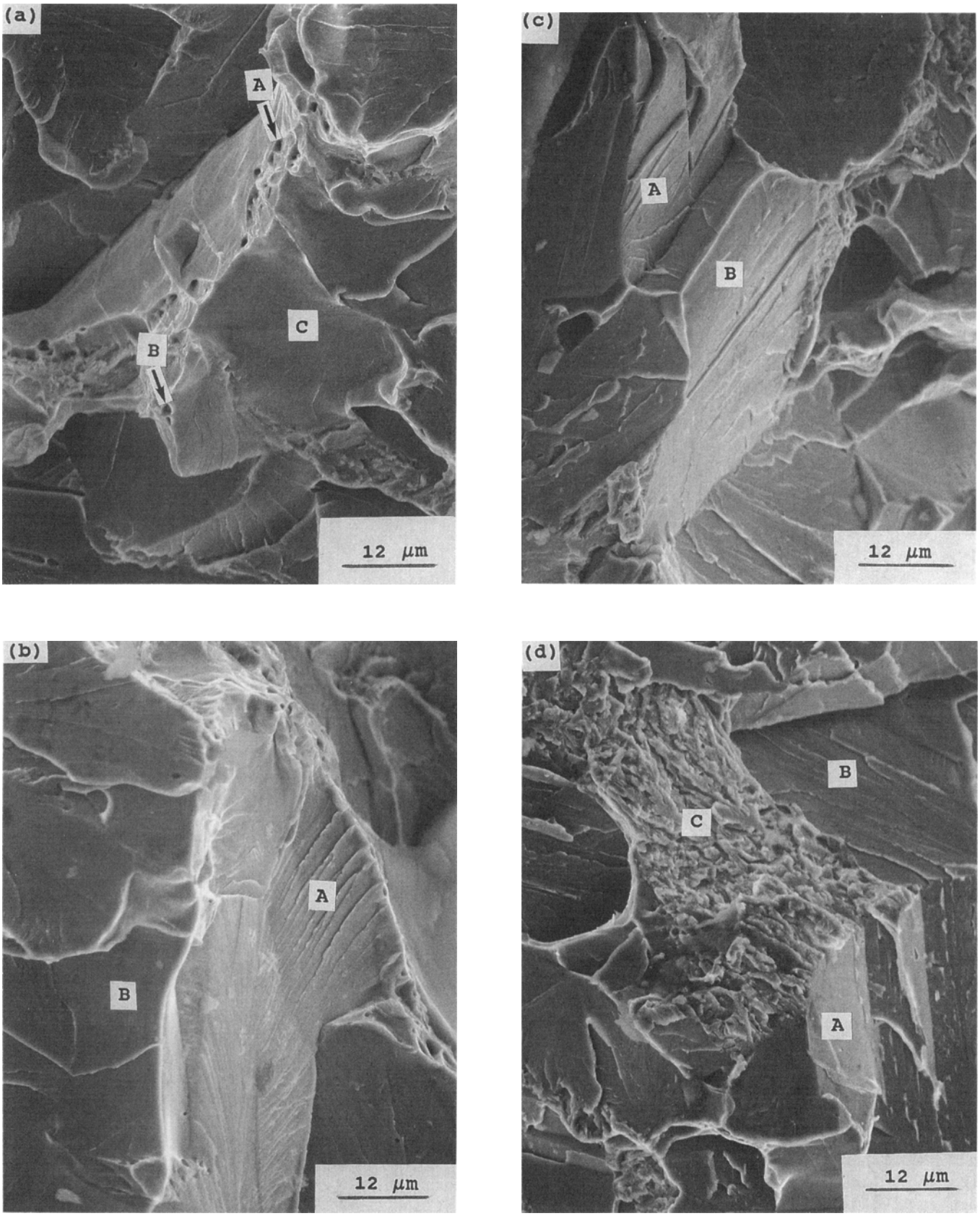

Fig. 13 Fractographs after Charpy impact tests at (a) 23 °C, (b) 0 °C, (c) –40 °C, and (d) –196 °C of material isothermally transformed at 700 °C for 0.5 h

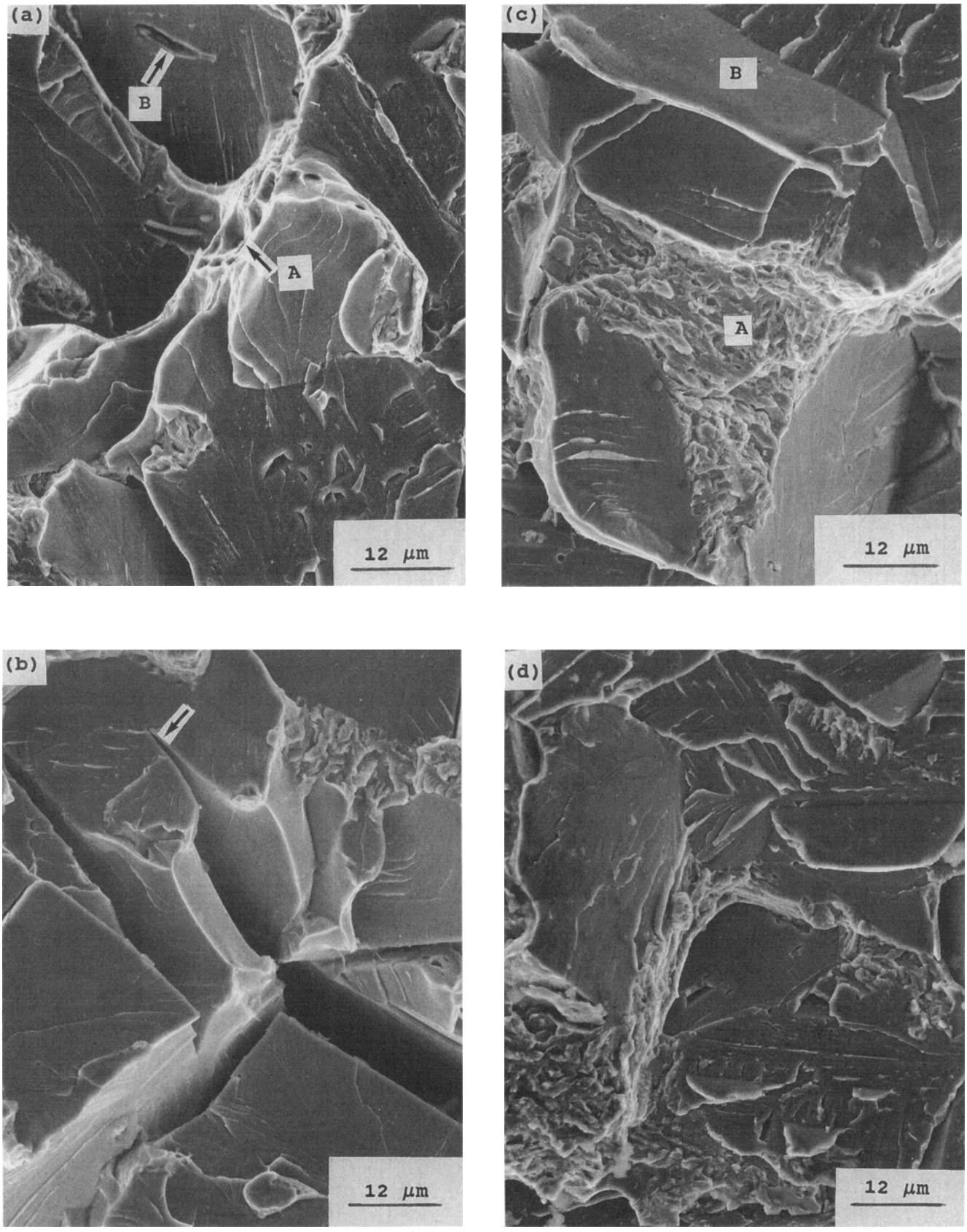

Fig. 14 Fractographs after Charpy impact tests at (a) 23 °C, (b) 0 °C, (c) –40 °C, and (d) –196 °C of material isothermally transformed at 700 °C for 2 h

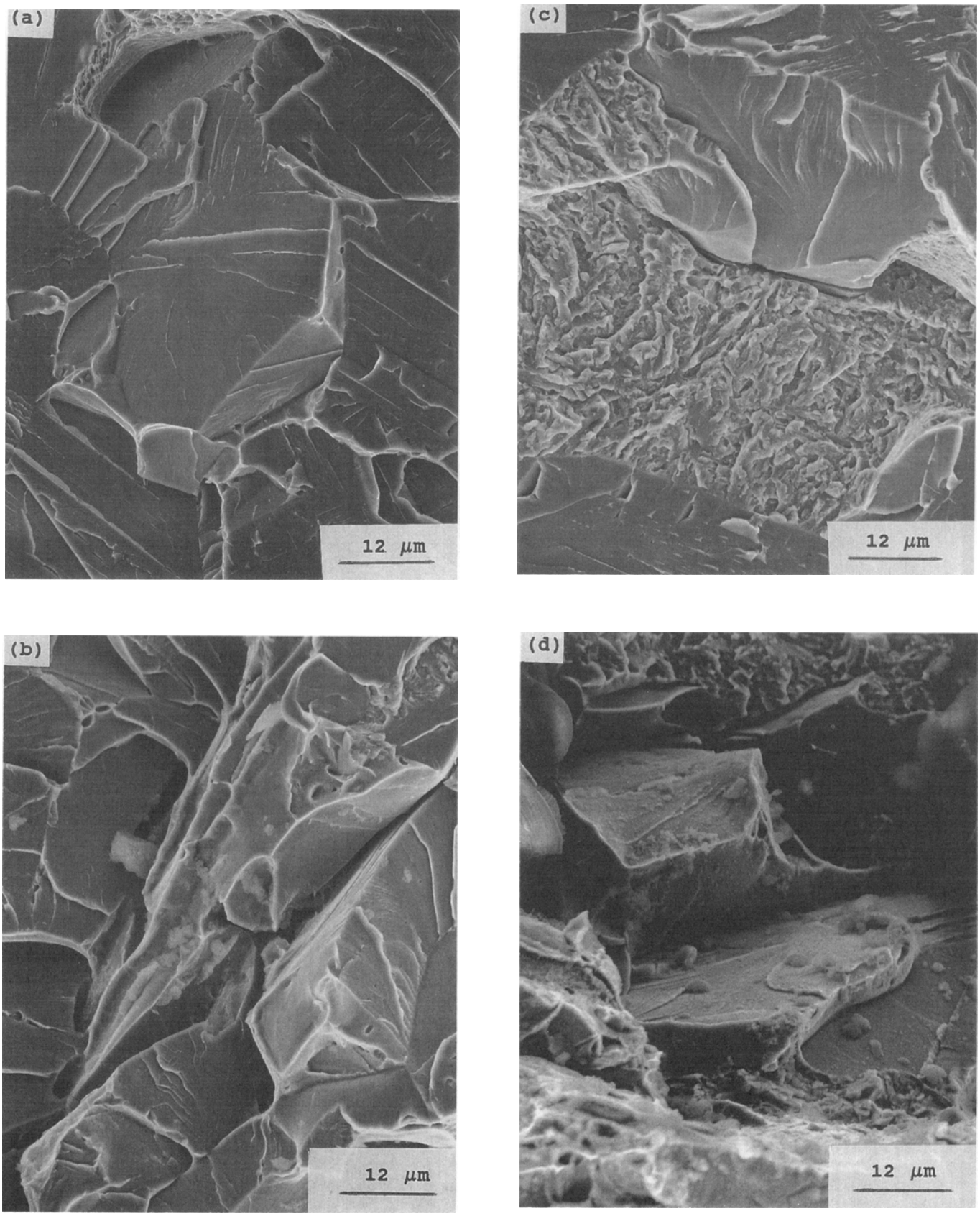

Fig. 15 Fractographs after Charpy impact tests at (a) 23 °C, (b) 0 °C, (c) –40 °C, and (d) –196 °C of material isothermally transformed at 700 °C for 8 h

coarsening of pearlite colonies and ferrite grain growth occurs during furnace cooling or isothermal transformation at 700 °C following austenitization at 1000 °C.

Acknowledgments

The author is grateful to the UNZA/DUT/MINENG project for financial support and to the Engineering Services Corporation (ESCO), Zambia, for donating the steel used in this work.

References

1. J. Yu and C.J. McMahon, Jr., Variation of the Fracture Mode in Temper Embrittled 2.25 Cr-1 Mo Steel, *Metall. Trans.*, Vol 16A, 1985, p 1325-1331
2. E. Tschegg and S. Stanzl, Fatigue Crack Propagation and Threshold in b.c.c. and f.c.c. Metals at 77 and 293 K, *Acta Metall.*, Vol 29, 1981, p 33-40
3. T.M. Maccagno and J.F. Knott, The Low Temperature Brittle Fracture Behaviour of Steel in Mixed Modes I and II, *Eng. Fract. Mech.*, Vol 38, 1991, p 111-128
4. X. Yan and W. Lei, Research into Fracture Behavior of Mild Steel in Crack-Like Notch Impact Test, *Scripta Met. Mater.*, Vol 29, 1993, p 797-800
5. A.R. Rosenfield and G.T. Hahn, Numerical Descriptions of the Ambient Low-Temperature, and High-Strain Rate Flow and Fracture Behavior of Plain Carbon Steel, *Trans. ASM*, Vol 59, 1966, p 962-980
6. D.A. Curry and J.F. Knott, Effects of Microstructure on Cleavage Fracture Stress in Steel, *Met. Sci.*, Vol 12, 1978, p 511-514
7. T. Lin, A.G. Evans, and R.O. Ritchie, Stochastic Modeling of the Independent Roles of Particle Size and Grain Size in Transgranular Cleavage Fracture, *Metall. Trans.*, Vol 18A, 1987, p 641-651
8. V. Tvergaard and A. Needleman, Effect of Material Rate Sensitivity on Failure Modes in the Charpy V-Notch Test, *J. Mech. Phys. Solids*, Vol 34, 1986, p 213-241
9. R.W. Balluffi and L.L. Seigle, Growth of Voids in Metals during Diffusion and Creep, *Acta Metall.*, Vol 5, 1957, p 449-454
10. J.A. Brinkman, Mechanism of Pore Formation Associated with the Kirkendall Effect, *Acta Metall.*, Vol 3, 1955, p 140-145
11. R.W. Bauer and H.G.F. Wilsdorf, Void Initiation in Ductile Fracture, *Scripta Metall.*, Vol 7, 1973, p 1213-1220
12. N.R. Moody and W.W. Gerberich, Fatigue Crack Propagation in Iron and Two Iron Binary Alloys at Low Temperatures, *Mater. Sci. Eng.*, Vol 41, 1979, p 271-280
13. F.B. Pickering and T. Gladman, "An Investigation into Some Factors Which Control the Strength of Carbon Steels," Special Report 81, Iron and Steel Institute, 1963
14. A. Needleman and V. Tvergaard, A Numerical Study of Void Distribution Effects on Dynamic, Ductile Crack Growth, *Eng. Fract. Mech.*, Vol 38, 1991, p 157-173
15. R. Becker, The Effect of Porosity Distribution on Ductile Failure, *J. Mech. Phys. Solids*, Vol 35, 1987, p 577-599
16. P.R. Frise and R. Bell, Fatigue Crack Growth and Coalescence at Notches, *Int. J. Fatigue*, Vol 14, 1992, p 51-56
17. J.H. Chen and C. Yan, Fracture Behaviour of C-Mn Steel Multipass MMA Weld Metals at –60 °C in Charpy V Testing, *Mater. Sci. Technol.*, Vol 4, 1988, p 732-739
18. S. Danyluk and I. Wolke, Low Temperature Impact Properties of Phosphorus and Sulfur Doped and Sensitized Type 304 Stainless Steel, *Metall. Trans.*, Vol 17A, 1986, p 663-668
19. E. Molinié, R. Piques, and A. Pineau, Behaviour of a 1Cr-1Mo-0.25V Steel after Long Term Exposure–I. Charpy Impact Toughness and Creep Properties, *Fatigue Fract. Eng. Mater. Struct.*, Vol 14, 1991, p 531-545
20. P. Bowen, S.G. Druce, and J.F. Knott, Micromechanical Modelling of Fracture Toughness, *Acta Metall.*, Vol 35, 1987, p 1735-1746